DAMAGE IDENTIFICATION IN PLATE STRUCTURES BASED ON THE TOPOLOGICAL DERIVATIVE METHOD

A.A.M. DA SILVA AND A.A. NOVOTNY

Abstract. In this work, a novel approach for solving a damage identification problem in plate structures based on the topological derivative method is proposed. The forward problems are governed by the elastodynamic Kirchhoff and Reissner-Mindlin plate bending models in the frequency domain. The inverse problem consists in finding a set of damages from pointwise domain measurements of the plate displacement field. The damage is represented by a variation in the plate thickness, which is assumed to be given by a piecewise constant function. A shape functional measuring the misfit between the available data (measurements) and the displacements computed from the model is minimized with respect to the geometrical support of the unknown damage distribution, by using the topological derivative method. Finally, some numerical experiments are presented, showing different features of the proposed approach in detecting and locating damages of varying sizes and shapes by taking into account noisy data.

1. Introduction

The identification of damages in their initial stage is of paramount importance in many physical and engineering problems. The damage process in structures may be catastrophic once it becomes out of control and could lead the structure to either a fail or even to the total collapse. Therefore, the continuous monitoring of the structure focusing in the identification of damages in the early stage promote important benefits, such as security for those who depend on it, reduced maintenance cost and increasing on the lifetime of the structure. In the work by Rytter (1993), the damage inspection methods are classified in four levels: detection of the presence of damage in the structure (level 1), location of the region affected by the damage (level 2), indication of the severity of the damage (level 3) and prediction of the remaining lifetime of the structure (level 4). In addition, damage identification methods based on dynamic tests are usually classified into four categories: time domain methods (Koh et al., 2003; Majumder and Manohar, 2003; Sandesh and Shankarb, 2009), frequency domain methods (Araújo dos Santos et al., 2005; Lee et al., 2003; Salawu and Williams, 1995), methods based on impedance (Liang et al., 1994; Park and Inman, 2007; Sun et al., 1995) and modal analysis (Corrêa et al., 2016; Stutz et al., 2005; Tenenbaum et al., 2013).

Important contributions in the damage inspection procedure have been reported in the literature. Many methods of damage location (level 2) are based on modifications of the flexibility matrix, the curvature of the vibration modes and the modal flexibility and the modal strain energy method, which are based on the vibration characteristics of the structure in the presence of damages (Bernal, 2002; Pandey and Biswas, 1994; Pandey et al., 1991; Shin et al., 2012; Tomaszewska, 2010). Optimization methods based on stochastic approaches have been successful applied for solving this class of problems. In the work by (Stutz et al., 2015), a comparative analysis between the Particle Swarm

Key words and phrases. Damage identification, Kirchhoff plate bending problem, Reissner-Mindlin plate bending problem, topological derivative method.

Optimization, Luus-Jaakola Optimization Method, Simulated Annealing Method, Particle Collision Method and Differential Evolution Method is presented. Hybridization between stochastic and deterministic optimization methods can be found in the papers by Begambre and Laier (2009); Tenenbaum et al. (2013). See also applications of Genetic Algorithms (Rao et al., 2004; Tenenbaum et al., 2013) and Neural Networks (Lee et al., 2005) in the structural damage quantification stage (level 3).

In this work, we propose a novel approach to simultaneously deal with structural damage detection (level 1) and location (level 2) based on the topological derivative method, which will be referred to as damage identification. The topological derivative concept, introduced in the fundamental paper by Sokołowski and Żochowski (1999), represents the sensitivity of a given shape functional with respect to the nucleation of an infinitesimal singular domain perturbation, such as holes, cracks or inclusions. The topological derivative method has applications in many different fields, including shape and topology optimization (Amstutz and Novotny, 2010; Novotny et al., 2007), inverse problems (Canelas et al., 2014; Ferreira and Novotny, 2017), image processing (Auroux et al., 2007; Belaid et al., 2008), fracture (Van Goethem and Novotny, 2010) and damage evolution modelling (Xavier et al., 2020). See also important contributions in the elastic-wave imaging problems (Guzina and Chikichev, 2007; Guzina and Pourahmadian, 2015; Tokmashev et al., 2013) and inverse scattering problems (Carpio and Rapún, 2008; Carpio and Rapún, 2012; Funes et al., 2016). The topological derivative method can be seen as a particular case of the broader class of asymptotic methods fully developed in the books by Ammari et al. (2013) and Ammari and Kang (2004), for instance. See also related works by Nazarov and Plamenevskij (1994); Maz'ya et al. (2000).

More precisely, we deal with damage detection and location in plate structures. The forward problems are governed by the elastodynamic Kirchhoff and Reissner-Mindlin plate bending models in the frequency domain. The inverse problem consists in finding a set of damages from pointwise domain measurements of the plate displacement field. The damage is represented by a variation in the plate thickness, which is assumed to be given by a piecewise constant function. Therefore, the damaged region to be reconstruct is characterised by a set of geometrical domains within the plate structure. The basic idea consists in minimizing the difference between the available data (measurements) and the displacements computed from the forward problem, with respect to a set of admissible geometrical domain representing the damage distribution, by using the topological derivative method.

This paper is organized as follows. In Section 2 the topological derivative is introduced for Kirchhoff (Section 2.1) and Reissner-Mindlin (Section 2.2) plate theories. The existence of the associated topological derivative is proved and the topological derivative is stated in its closed form. Some numerical experiments are presented in Section 3, showing different features of the proposed approach in detecting and locating damages of varying sizes and shapes by taking into account noisy data. Finally, the paper ends with some concluding remarks in Section 4.

2. The Topological Derivative Method

In this Section, we present the topological derivative method in the context of damage identification in plate structures. We start by introducing the definition of the topological derivative itself. Therefore, let us consider an open and bounded domain $D \subset \mathbb{R}^2$ which is subject to a non-smooth perturbation confined in a small ball $B_\varepsilon(\hat{x})$ of size ε and center at $\hat{x} \in D$, with $\overline{B_\varepsilon(\hat{x})} \subset D$. We also introduce a characteristic function $x \mapsto \chi(x)$ associated

to the unperturbed domain, namely $\chi = \mathbb{1}_D$ such that

$$|D| = \int_D \chi, \tag{2.1}$$

where $|D|$ is the Lebesgue measure of D. The characteristic function associated with the topological perturbed domain is defined by the mapping $x \mapsto \chi_\varepsilon(\hat{x}; x)$, $x \in \mathbb{R}^2$. In the case of a perforation, for instance, $\chi_\varepsilon(\hat{x}) = \mathbb{1}_D - \mathbb{1}_{B_\varepsilon(\hat{x})}$, so that the topologically perturbed domain is obtained as $D_\varepsilon = D \setminus \overline{\omega_\varepsilon}$. Finally, we assume that a given shape functional $\psi(\chi_\varepsilon(\hat{x}))$, associated with the topologically perturbed domain, admits a topological asymptotic expansion of the form

$$\psi(\chi_\varepsilon(\hat{x})) = \psi(\chi) + f(\varepsilon)\mathcal{T}(\hat{x}) + o(f(\varepsilon)), \tag{2.2}$$

where $\psi(\chi)$ is the shape functional associated to the unperturbed domain, $f(\varepsilon)$ is a positive function such that $f(\varepsilon) \to 0$, with $\varepsilon \to 0$, and $o(f(\varepsilon))$ is the remainder. The function $\hat{x} \to \mathcal{T}(\hat{x})$ is then defined as the topological derivative of ψ at $\hat{x}$. For more details, see for instance the book by Novotny and Sokołowski (2020).

Let us consider a plate represented by a two-dimensional domain $D \subset \mathbb{R}^2$ as shown in Figure 1. We assume that the boundary of D, denoted by ∂D, is a curvilinear polygon of class $\mathcal{C}^{1,1}$ (Amstutz and Novotny, 2011). The damage is represented by a variation in the plate thickness, which is assumed to be given by a piecewise constant function of the form

$$h(x) := \begin{cases} h_0, \text{ if } x \in \Omega, \\ h_1, \text{ if } x \in \omega, \end{cases} \tag{2.3}$$

where $h_0 > 0$ is assumed to be constant and $h_1 = h_1(x)$ is a positive piecewise constant function such that $h_1 < h_0$ in D, and $D = \Omega \cup \omega$, with $\Omega \cap \omega = \varnothing$. Therefore, Ω represents the healthy part of D whereas ω is the damaged region. Note that the smaller thickness h_1 is used to represent loss of stiffness and mass caused by delamination or corrosion, for example, but not necessary a reduction on the thickness itself.

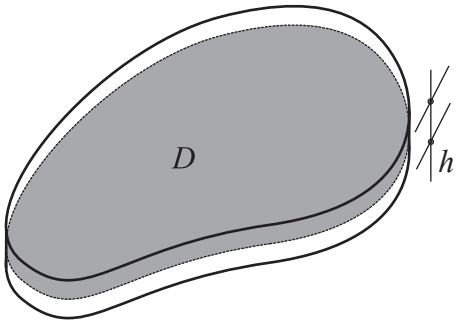

FIGURE 1. The working domain from the paper by Amstutz and Novotny (2011).

The inverse problem we are dealing with consists in finding the damaged distribution from pointwise measurement of the plate displacement. We assume that h_0 and h_1 are given, so that we have to find the support of the damage region $\omega^\star$ associated with $h^\star$ according to (2.3). We will show later that this assumption can be weakened.

Since the unknown is now given by a geometrical domain ω, then the inverse problem can be written in the form of a topology optimization problem. More precisely, we want

to minimize a shape functional measuring the misfit between the available data (measurement) and the solution computed from the model problem, with respect to the support ω of the damaged region, namely

$$\underset{\omega \subset D}{\text{Minimize}}\ \mathcal{J}(u,\theta). \tag{2.4}$$

The shape functional $\mathcal{J}(u,\theta)$ is defined as

$$\mathcal{J}(u,\theta) = \sum_{i=1}^{N} \int_D (|u-u^*|^2 + \|\theta-\theta^*\|^2)\delta(x-x_i), \tag{2.5}$$

where $\delta(x,x_i)$ is the Dirac delta function with pole at $x_i \in D$, $u : D \to \mathbb{R}$ and $\theta : D \to \mathbb{R}^2$ are the transverse displacement and rotation vector field of the plate, respectively, according to the model problem we are dealing with. In addition, (u^*,θ^*) is the pointwise measurement of the plate displacement and x_i, $i = 1,\cdots,N$, represent the locations of the sensors (accelerometers), with N the number of sensors.

A quite general approach to deal with the resulting topology optimization problem is based on the topological derivative method (Novotny and Sokołowski, 2013, 2020). In the context of this work, the topological derivative represents the sensitivity of the misfit shape functional with respect to the introduction of a perturbation of size ε and center at an arbitrary point $\hat{x} \in D$ representing a small ball-shaped damaged region $B_\varepsilon(\hat{x}) \subset D$. The perturbed counterpart of the plate thickness h is denoted as $h_\varepsilon = \gamma_\varepsilon h$, with

$$\gamma_\varepsilon(x) := \begin{cases} 1, \text{ if } x \in D \setminus B_\varepsilon(\hat{x}), \\ \gamma, \text{ if } x \in B_\varepsilon(\hat{x}), \end{cases} \tag{2.6}$$

where $\gamma = \gamma(x)$ is used to denote the contrast in the plate thickness, namely

$$\gamma(x) := \begin{cases} h_1/h_0, \text{ if } x \in \Omega, \\ h_0/h_1, \text{ if } x \in \omega, \end{cases} \tag{2.7}$$

remembering that $\Omega = D \setminus \omega$ and ω are used to represent the healthy and damaged regions of the plate, respectively. From these elements, two topological perturbations are possible. If $\overline{B_\varepsilon(\hat{x})} \subset \Omega$, then $h_\varepsilon = h_0$ in $\Omega \setminus B_\varepsilon(\hat{x})$ and $h_\varepsilon = h_1$ in $B_\varepsilon(\hat{x}) \cup \omega$. Otherwise, if $\overline{B_\varepsilon(\hat{x})} \subset \omega$, then $h_\varepsilon = h_1$ in $\omega \setminus B_\varepsilon(\hat{x})$ and $h_\varepsilon = h_0$ in $B_\varepsilon(\hat{x}) \cup \Omega$. These general situations are considered for the sake of completeness. However, we are interested in the particular case in which $h = h_0$ in D, so that $h_\varepsilon = h_0$ in $D \setminus B_\varepsilon(\hat{x})$ and $h_\varepsilon = h_1$ in $B_\varepsilon(\hat{x})$. We will come back to this discussion in Section 3.

According to (2.6), the perturbed counterpart of the shape functional is given by

$$\mathcal{J}(u_\varepsilon,\theta_\varepsilon) = \sum_{i=1}^{N} \int_D (|u_\varepsilon-u^*|^2 + \|\theta_\varepsilon-\theta^*\|^2)\delta(x-x_i), \tag{2.8}$$

for $x_i \notin B_\varepsilon(\hat{x})$, $i = 1,\cdots,N$, where $u_\varepsilon : D \to \mathbb{R}$ and $\theta_\varepsilon : D \to \mathbb{R}^2$ are the transverse displacement and rotation vector field of the plate, respectively, associated with the perturbed counterpart of the model problem we are dealing with. Finally, let us introduce the following fourth-order polarization tensor associated with the plate bending model

$$\mathbb{P}_\gamma = -\frac{1-\gamma^3}{1+\gamma^3\beta}\left((1+\beta)\mathbb{I} + \frac{1-\gamma^3}{2}\frac{\alpha-\beta}{1+\gamma^3\alpha}\mathrm{I}\otimes\mathrm{I}\right), \tag{2.9}$$

where the symbols $\mathbb{I}$ and I are used to denote the second and fourth order identity tensor, respectively. The coefficients α and β will be defined later according to the model problem we are dealing with, either Kirchhoff or Reissner-Mindlin.

2.1. **Kirchhoff problem.** The theory of Kirchhoff plates is based on the kinematic assumption in which the normal fibers to the middle plane of the plate remain normal during deformation and do not suffer variations in their length. Therefore, both transverse shear and normal deformations are null. The transverse displacement (or deflection) of the plate in the time harmonic regime written in the frequency domain is solution to the following variational problem:

$$u \in \mathcal{U} : \int_D h^3 \mathcal{M}(u) \cdot \nabla\nabla\eta - k^2 \int_D hu\eta = \int_D b\eta \quad \forall \eta \in \mathcal{U}, \tag{2.10}$$

where k is the wave number defined as $k^2 = \rho(2\pi f)^2$, with f the working frequency and ρ the material density, h is the plate thickness, b is the source-term, $u : D \to \mathbb{R}$ is the transverse displacement and $\theta = \nabla u$ is the rotation. In addition, $\mathcal{M}(u)$ the moment tensor, namely

$$\mathcal{M}(u) = \frac{E}{12(1-\nu^2)}[(1-\nu)\mathbb{I} + \nu \mathrm{I} \otimes \mathrm{I}]\nabla\nabla u, \tag{2.11}$$

with I and $\mathbb{I}$ used to denote the second and fourth order identity tensors, respectively, whereas E is the Young modulus and ν is the Poisson ratio. The set of kinematically admissible displacements $\mathcal{U}$ is defined as

$$\mathcal{U} := \{\varphi \in H^2(D) : \varphi_{|\partial D} = 0\}. \tag{2.12}$$

Note that, from (2.12), the plate is assumed to be simply supported on ∂D. According to (2.6), the perturbed counterpart of the variational problem (2.10) reads

$$u_\varepsilon \in \mathcal{U} : \int_D h_\varepsilon^3 \mathcal{M}(u_\varepsilon) \cdot \nabla\nabla\eta - k^2 \int_D h_\varepsilon u_\varepsilon \eta = \int_D b\eta \quad \forall \eta \in \mathcal{U}. \tag{2.13}$$

Finally, we assume that the quantity k^2 is neither an eigenvalue of (2.10) nor (2.13).

2.1.1. *Existence of the topological derivative.* The existence of the topological derivative associated with the problem we are dealing with is ensured by the following result:

Lemma 1. *Let u and u_ε be the solutions of the variational problems* (2.10) *and* (2.13)*, respectively. Then, the following a priori estimate holds true*

$$\|u_\varepsilon - u\|_{H^2(D)} \leq C\varepsilon, \tag{2.14}$$

with constant C independent of the small parameter ε.

Proof. Let us rewrite the variation problem (2.10) using the definition for the contrast (2.6) as follows

$$\int_D h_\varepsilon^3 \mathcal{M}(u) \cdot \nabla\nabla\eta - k^2 \int_D h_\varepsilon u\eta = (\gamma^3 - 1) \int_{B_\varepsilon} h^3 \mathcal{M}(u) \cdot \nabla\nabla\eta - k^2(\gamma - 1) \int_{B_\varepsilon} hu\eta + \int_D b\eta. \tag{2.15}$$

After subtracting (2.15) from (2.13), we have

$$\int_D h_\varepsilon^3 \mathcal{M}(\tilde{u}_\varepsilon) \cdot \nabla\nabla\eta - k^2 \int_D h_\varepsilon \tilde{u}_\varepsilon \eta = (1-\gamma^3) \int_{B_\varepsilon} h^3 \mathcal{M}(u) \cdot \nabla\nabla\eta - k^2(1-\gamma) \int_{B_\varepsilon} hu\eta, \tag{2.16}$$

where $\tilde{u}_\varepsilon = u_\varepsilon - u$. Let us consider a decomposition of the form $\tilde{u}_\varepsilon = v_\varepsilon + w_\varepsilon$. Then $v_\varepsilon \in \mathcal{U}$ is solution to

$$\int_D h_\varepsilon^3 \mathcal{M}(v_\varepsilon) \cdot \nabla\nabla\eta = (1-\gamma^3) \int_{B_\varepsilon} h^3 \mathcal{M}(u) \cdot \nabla\nabla\eta - k^2(1-\gamma) \int_{B_\varepsilon} hu\eta, \tag{2.17}$$

whereas $w_\varepsilon \in \mathcal{U}$ is solution to

$$\int_D h_\varepsilon^3 \mathcal{M}(w_\varepsilon) \cdot \nabla\nabla\eta - k^2 \int_D h_\varepsilon(w_\varepsilon)\eta = k^2 \int_D h_\varepsilon v_\varepsilon \eta. \tag{2.18}$$

By taking into account the well-posedness of the variational problem (2.18), we obtain (Monk, 2003)

$$\|w_\varepsilon\|_{H^2(D)} \leq C_1 \|v_\varepsilon\|_{L^2(D)} \leq C_1 \|v_\varepsilon\|_{H^2(D)}. \tag{2.19}$$

On the other hand, by setting $\eta = v_\varepsilon$ as test function in the variational problem (2.17), there is

$$\int_D h_\varepsilon^3 \mathcal{M}(v_\varepsilon) \cdot \nabla\nabla v_\varepsilon = (1-\gamma^3) \int_{B_\varepsilon} h^3 \mathcal{M}(u) \cdot \nabla\nabla v_\varepsilon - k^2(1-\gamma) \int_{B_\varepsilon} huv_\varepsilon. \tag{2.20}$$

From the Poincaré inequality (Quarteroni and Valli, 1997), it follows

$$c\|v_\varepsilon\|^2_{H^2(D)} \leq \int_D h_\varepsilon^3 \mathcal{M}(v_\varepsilon) \cdot \nabla\nabla v_\varepsilon. \tag{2.21}$$

Therefore, we get

$$\|v_\varepsilon\|^2_{H^2(D)} \leq C_2 \left[(1-\gamma^3) \int_{B_\varepsilon} h^3 \mathcal{M}(u) \cdot \nabla\nabla v_\varepsilon - k^2(1-\gamma) \int_{B_\varepsilon} huv_\varepsilon \right] \tag{2.22}$$

with $C_2 = 1/c$. After applying the Cauchy-Schwartz inequality (Quarteroni and Valli, 1997), there is

$$\|v_\varepsilon\|^2_{H^2(D)} \leq C_3 \varepsilon \|\nabla\nabla v_\varepsilon\|_{L^2(B_\varepsilon)} + C_4 \varepsilon \|v_\varepsilon\|_{L^2(B_\varepsilon)} \leq C_5 \varepsilon \|v_\varepsilon\|_{H^2(D)}. \tag{2.23}$$

Finally, from the triangular inequality in $\tilde{u}_\varepsilon = v_\varepsilon + w_\varepsilon$ combined with the estimates (2.19) and (2.23), we obtain the required result, namely

$$\|\tilde{u}_\varepsilon\|_{H^2(D)} = \|w_\varepsilon + v_\varepsilon\|_{H^2(D)} \leq \|w_\varepsilon\|_{H^2(D)} + \|v_\varepsilon\|_{H^2(D)} \leq C\varepsilon, \tag{2.24}$$

with $C = (1 + C_1)C_5$ independent of the small parameter ε. □

2.1.2. *Topological derivative formula.* By setting the constants α and β in the definition of the polarization tensor (2.9) as follows

$$\alpha = \frac{1+\nu}{1-\nu} \quad \text{and} \quad \beta = \frac{1-\nu}{3+\nu}, \tag{2.25}$$

we can present the main result of this section, namely:

Theorem 2. *The topological derivative of the tracking-type shape functional $\mathcal{J}(u,\theta)$ from (2.5), where $\theta = \nabla u$, with respect to the nucleation of a small damage represented by a piecewise constant variation in the plate thickness, is given by*

$$\mathcal{T}(x) = h^3 \mathbb{P}_\gamma \mathcal{M}(u) \cdot \nabla\nabla v(x) + k^2(1-\gamma) huv(x), \quad \forall x \in D \setminus \{x_1, \cdots, x_N\}, \tag{2.26}$$

where u is solution to (2.10), k is the wave number, h is the plate thickness and γ its contrast. The polarization tensor $\mathbb{P}_\gamma$ is defined by (2.9) together with the coefficients α and β according to (2.25). Moreover, function v is solution to the following adjoint problem: Find $v \in \mathcal{U}$, such that

$$\int_D h^3 \mathcal{M}(v) \cdot \nabla\nabla\eta - k^2 \int_D hv\eta = 2 \sum_{i=1}^{N} \int_D \delta(x - x_i)[(u - u^*)\eta + (\nabla u - \theta^*) \cdot \nabla\eta] \quad \forall \eta \in \mathcal{U}, \tag{2.27}$$

where (u^*, θ^*) is the target obtained from pointwise measurement of the plate displacement. Finally, we assume that the quantity k^2 is not an eigenvalue of problem (2.27).

Proof. The proof of this result follows the same steps as presented in the paper by (Amstutz and Novotny, 2011) combined with the reasoning used in the proof of Lemma 1, since we are dealing with a non-coercive counterpart of the problem considered in the work by (Amstutz and Novotny, 2011). □

2.2. **Reissner-Mindlin problem.** The Reissner-Mindlin problem is based on the kinematic assumption that the normal fibers to the middle plane of the plate remain straight during the deformation process and do not suffer variations in the length, but they not necessarily remain normal to the middle plane. Consequently, the transverse shear deformations are not negligible and the normal deformations are null. By neglecting the rotational inertia effects, the transverse displacement and rotations of the plate in the time harmonic regime written in the frequency domain is solution to the following variational problem: Find $(\theta, u) \in \mathcal{U}$, such that

$$\int_D h^3 \mathcal{M}(\theta) \cdot (\nabla\varphi)^s + \int_D hQ(\theta, u) \cdot (\varphi - \nabla\eta) - k^2 \int_D hu\eta = \int_D b\eta \quad \forall (\varphi, \eta) \in \mathcal{U}, \quad (2.28)$$

where k is the wave number defined as $k^2 = \rho(2\pi f)^2$, with f the working frequency and ρ the material density, h is the plate thickness, b is the source-term, $u : D \to \mathbb{R}$ is the transverse displacement and $\theta : D \to \mathbb{R}^2$ is the rotation vector field. In addition, $M(\theta)$ is the generalized bending moment tensor and $Q(\theta, u)$ is the generalized shear tensor given, respectively, by

$$\mathcal{M}(\theta) = \frac{E}{12(1-\nu^2)}[(1-\nu)\mathbb{I} + \nu \mathrm{I} \otimes \mathrm{I}](\nabla\theta)^s \quad (2.29)$$

and,

$$Q(\theta, u) = \frac{5E}{12(1+\nu)}(\theta - \nabla u), \quad (2.30)$$

with I and $\mathbb{I}$ used to denote the second and fourth order identity tensors, respectively, whereas E is the Young modulus and ν is the Poisson ratio. The set of kinematically admissible displacements $\mathcal{U}$ is defined as

$$\mathcal{U} := \{(\phi, \varphi) \in H^1(D, \mathbb{R}^2) \times H^1(D) : \varphi_{|\partial D} = 0\}. \quad (2.31)$$

Note that, from (2.31), the plate is assumed to be simply supported ∂D. According to (2.6), the perturbed counterpart of the variation problem (2.28) reads: Find $(\theta_\varepsilon, u_\varepsilon) \in \mathcal{U}$, such that

$$\int_D h_\varepsilon^3 \mathcal{M}(\theta_\varepsilon) \cdot (\nabla\varphi)^s + \int_D h_\varepsilon Q(\theta_\varepsilon, u_\varepsilon) \cdot (\varphi - \nabla\eta) - k^2 \int_D h_\varepsilon u_\varepsilon \eta = \int_D b\eta \quad \forall (\varphi, \eta) \in \mathcal{U}. \quad (2.32)$$

Finally, we assume that the quantity k^2 is neither an eigenvalue of (2.28) nor (2.32).

2.2.1. *Existence of the topological derivative.* The existence of the topological derivative associated with the problem we are dealing with is ensured by the following result:

Lemma 3. *Let (θ, u) and $(\theta_\varepsilon, u_\varepsilon)$ be the solutions of the variational problems* (2.28) *and* (2.32)*, respectively. Then, the following a priori estimates hold true*

$$\|\theta_\varepsilon - \theta\|_{H^1(D,\mathbb{R}^2)} \leq C_1 \varepsilon \quad \text{and} \quad \|u_\varepsilon - u\|_{H^1(D)} \leq C_2 \varepsilon, \quad (2.33)$$

with constants C_1 and C_2 independent of the small parameter ε.

Proof. The demonstration of these results follows the same arguments as in the proof of Lemma 1. □

2.2.2. *Topological derivative formula.* Now, let us set the constants α and β in the definition of the polarization tensor (2.9) as follows

$$\alpha = \frac{1+\nu}{1-\nu} \quad \text{and} \quad \beta = \frac{3-\nu}{1+\nu}. \tag{2.34}$$

Then we can present the main result of this section, which is stated as:

Theorem 4. *The topological derivative of the tracking-type shape functional $\mathcal{J}(u,\theta)$ from (2.5), with respect to the nucleation of a small damage represented by a piecewise constant variation in the plate thickness, is given by*

$$\mathcal{T}(x) = h^3 \mathbb{P}_\gamma M(\theta) \cdot (\nabla\phi)^s(x) + hP_\gamma Q(\theta,u) \cdot (\phi - \nabla v)(x) + hk^2(1-\gamma)uv(x), \tag{2.35}$$

for all $x \in D \setminus \{x_1, \cdots, x_N\}$, where (θ, u) is solution to (2.28), k is the wave number, h is the plate thickness and γ its contrast. The fourth-order polarization tensor $\mathbb{P}_\gamma$ is defined by (2.9) together with the coefficients α and β according to (2.34). In addition, the second-order polarization tensor P_γ is given by

$$P_\gamma = -2\frac{1-\gamma}{1+\gamma}\mathrm{I}. \tag{2.36}$$

Moreover, function v is solution to the following adjoint problem: Find $(\phi, v) \in \mathcal{U}$, such that

$$\int_D h^3 M(\phi)\cdot(\nabla\varphi)^s + \int_D hQ(\phi,v)\cdot(\varphi - \nabla\eta) - k^2\int_D hv\eta = 2\sum_{i=1}^{N}\int_D \delta(x-x_i)[(u-u^*)\eta + (\theta-\theta^*)\cdot\varphi] \quad \forall(\varphi,\eta)\in\mathcal{H}(D), \tag{2.37}$$

where (u^*, θ^*) is the target obtained from pointwise measurement of the plate displacement. Finally, we assume that the quantity k^2 is not an eigenvalue of problem (2.37).

Proof. The proof of this result follows the same steps as presented in the paper by Sales et al. (2015) combined with the reasoning used in the proof of Lemma 1, since we are dealing with a non-coercive counterpart of the problem considered in the work by Sales et al. (2015). □

3. Numerical Results

By setting $\omega = \varnothing$, the solutions to the model problems and the associated topological derivatives are evaluated in the homogeneous domain with uniform thickness h_0, free of any anomaly. On the other hand, in order to produce synthetic data, the measurements (u^*, θ^*) are obtained as solutions to the model problems defined in the heterogeneous domain with thickness $h^\star$ by setting $\omega = \omega^\star$, where $\omega^\star$ is the support of the true anomalies we are looking for. More details will be given later on while setting the numerical experiments.

Note that in order to use the results from Theorems 2 and 4 for solving the inverse problem we are dealing with, it is necessary to know the contrast γ from (2.7) a priori. It means to know how much the plate is damaged. However, this information in general is not available. In order to deal with this more difficult scenario, we take $\gamma \to 0$ (or equivalently $h_1 \to 0$, provided that $h = h_0$ ($\omega = \varnothing$) and $h_1 < h_0$) in Theorems 2 and 4 and use the obtained results for solving the minimization problem (2.4) by considering the sensitivity associated with $h_1 \to 0$. More precisely, we have:

Corollary 5. *For $h = h_0$, the limit case $\gamma \to 0$ ($h_1 \to 0$) in (2.26) is well defined and given by*

$$\mathcal{T}(x) = h_0^3 \mathbb{P}_0 \mathcal{M}(u) \cdot \nabla\nabla v(x) + k^2 h_0 uv(x), \quad \forall x \in D \setminus \{x_1, \cdots, x_N\}, \tag{3.1}$$

where the polarization tensor $\mathbb{P}_0$ is written as

$$\mathbb{P}_0 = \frac{-1}{3+\nu}\left(4\mathbb{I} + \frac{1+3\nu}{1-\nu}\mathrm{I}\otimes\mathrm{I}\right). \tag{3.2}$$

Corollary 6. *For $h = h_0$, the limit case $\gamma \to 0$ ($h_1 \to 0$) in (2.35) is well defined and given by*

$$\mathcal{T}(x) = h_0^3 \mathbb{P}_0 M(\theta) \cdot (\nabla\phi)^s(x) - 2h_0 Q(\theta, u) \cdot (\phi - \nabla v)(x) + h_0 k^2 uv(x), \tag{3.3}$$

for all $x \in D \setminus \{x_1, \cdots, x_N\}$, where the polarization tensor written as

$$\mathbb{P}_0 = \frac{-1}{1+\nu}\left(4\mathbb{I} - \frac{1-3\nu}{1-\nu}\mathrm{I}\otimes\mathrm{I}\right). \tag{3.4}$$

The basic idea consists in plotting the topological derivative field $\mathcal{T}(x)$ according to Corollaries 5 and 6. It is expected that the more $\mathcal{T}(x)$ is negative, the more likely $x \in D$ is within the damage region $\omega^\star \subset D$, given qualitative information on the detection and location of the damaged zone.

Based on the former discussion, in this section some numerical experiments are presented. The objective is to show different features of the proposed method when solving the inverse problem of damage location in plate structure. We consider a simply supported square-shaped plate of dimensions $(1 \times 1)\mathrm{m}^2$. The wave number is defined as $k^2 = \rho(2\pi f)^2$, where ρ is the material density and f is the working frequency to be defined later. The physical material properties of the plate made with steel are Young Modulus $E = 210\mathrm{GPa}$, Poisson ratio $\nu = 0.3$ and density $\rho = 7800\mathrm{kg/m}^3$. We consider synthetic data produced numerically. More precisely, the background thickness is set as $h_0 = 0.01\mathrm{m}$ whereas the damaged region $\omega^\star$ has thickness $h_1(x) < h_0$ to be specified later on, inducing loss of mass and stiffness of the plate.

In the identification process, we consider a number M of measurements produced by pointwise sources $b_j(x) = b_0\delta(x - x_j)$, where $b_0 = 10^2\mathrm{N}$ is the source intensity and $x_j \in D$ are their locations, with $j = 1, \cdots, M$. More precisely, a concentrated transverse load is applied at the point x_j and the associated measurement (u_j^*, θ_j^*) is obtained. Then, the shape functional to be minimized is given by the sum

$$\mathcal{J}((u_1, \theta_1), \cdots, (u_M, \theta_M)) = \sum_{i=1}^{N}\sum_{j=1}^{M}\int_D (|u_j - u_j^*|^2 + \|\theta_j - \theta_j^*\|^2)\delta(x - x_i), \tag{3.5}$$

where (u_j, θ_j) is the plate displacement field obtained by setting $b = b_j$ in (2.10) or (2.28), according to the model problem we are dealing with. The associated topological derivatives are then obtained simply by the sum of the contribution of each measurement.

The target (u_j^*, θ_j^*) is evaluated as a restriction at the points $x_i \in D$, $i = 1, \cdots, N$, of the solution to (2.10) or (2.28) for $b = b_j$, by considering different configurations of the damage $\omega^\star$, where x_i represent the locations of the sensors. Moreover, by setting $\omega = \varnothing$, the displacement field (u_j, θ_j) is obtained after solving (2.10) and (2.28) for $b = b_j$ and $h = h_0$, uniform.

In addition, we consider multi-frequency approach as proposed in the papers by Park (2013) and Park (2017). More precisely, we follow the ideas introduced in the works by

Louër and Rapún (2019) and Pena and Rapún (2020), which consist in defining a weighted topological derivative in the form

$$\mathcal{T}^*(x) = \sum_{\ell=1}^{N_f} \mu_\ell \mathcal{T}_\ell(x), \tag{3.6}$$

where N_f is the number of frequencies, $\mathcal{T}_\ell(x)$ is the topological derivative associated with the ℓ-th frequency and μ_ℓ is the weight computed as

$$\mu_\ell = \left| \min_{x \in D} \mathcal{T}_\ell(x) \right|^{-1}. \tag{3.7}$$

The directs (2.10,2.28) and adjoints (2.27,2.37) problems are solved numerically by using the Finite Element Method according to Batoz (1982) and Katili (1993) for Kirchhoff and Reissner-Mindlin plate bending problems, respectively. More precisely, the square-shaped plate is split into 100 uniform squares. Then, each smaller square is divided into 4 identical triangles. In order to fulfill the Ihlenburg-Babuška condition (Ihlenburg and Babuška, 1995), each triangle is divided into 4 more triangles in such a way that the initial pattern is preserved. This procedure is repeated three times, leading to 25600 triangles. The resulting mesh is then used to discretize the boundary value problems.

Since we are considering synthetic data, in order to alleviate the so-called *inverse crime*, eventually the target (u_j^*, θ_j^*) is computed in a finer mesh obtained after repeating the last step of the above procedure two more times, leading to 409600 elements. At the same time, the measurements are corrupted with White Gaussian Noise (WGN). In practice, several external factors may generate significant changes in the dynamic response of the accelerometers used to measure the data (u_j^*, θ_j^*), such as acoustic noise, temperature variations and humidity. Therefore, noisy data in our context can be interpreted as uncertainties in the displacement measurements and the finer mesh is used to represent modeling inaccuracy. Finally, we consider $M = 64$ pointwise sources according to Figure 2(a). A number of $N = 24$ or $N = 69$ accelerometers are distributed either as in Figure 2(b) or Figure 2(c), respectively, depending on the example to be presented.

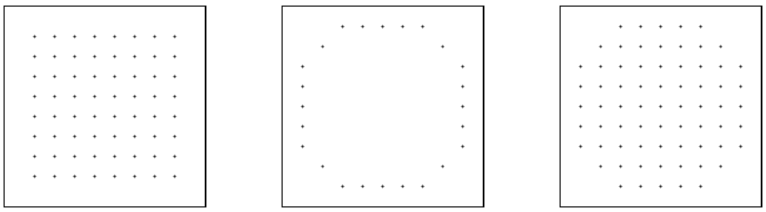

(a) (b) (c)

FIGURE 2. Pointwise source locations (a) and two accelerometers configurations with 24 points (b) and 69 points (c).

In summary, we consider four numerical examples. The pointwise sources distribution as in Figure 2(a) are used in all of them. In Examples 1-3, a number of 24 accelerometers is considered according to Figure 2(b). In Example 4, we consider 69 accelerometers as shown in Figure 2(c). The working frequency is set in the range from 4Hz to 180Hz, with increment of 4Hz, so that the number of frequencies in (3.6) is given by $N_f = 45$ for all examples.

3.1. **Example 1: Identification of two simultaneous damages of different sizes endowed with very low contrast.** In this first example, we consider the identification of two simultaneous circular damages of different sizes endowed with low contrast ($\gamma = 0.99$). The bigger damage of radius 0.04m is centered at $(0.40, 0.60)$, whereas the smaller damage with radius 0.02m is centered at $(0.70, 0.40)$, as shown in Figure 3. The resulting topological derivative fields $\mathcal{T}^*(x)$ are presented in Figures 4(a) and 4(b) for Kirchhoff and Reinssner-Midlin plate models, respectively. From an analysis of these figures, we observe that the topological derivative is more negative in the neighborhood of the hidden damages, as expected. The bigger damage is more evident as also expected.

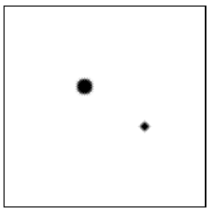

FIGURE 3. Example 1: Target $\omega^\star$ to be reconstructed given by two simultaneous circular damages with radii 0.04m and 0.02m at the positions $(0.40, 0.60)$ and $(0.70, 0.40)$, respectively, both endowed with contrast $\gamma = 0.99$.

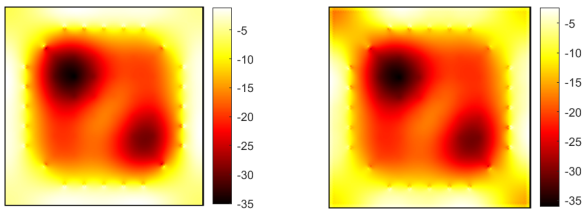

(a) (b)

FIGURE 4. Example 1: Obtained result for Kirchhoff (a) and Reissner-Mindlin (b) plate models by considering 24 sensors distributed as in Figure 2(b).

3.2. **Example 2: Identification of two simultaneous damages of same sizes endowed with different contrasts.** In this example we deal with the identification of two simultaneous circular damages of the same sizes and different contrasts. In particular, the damages have radius 0.02m and centers at $(0.40, 0.60)$ and $(0.70, 0.40)$ with contrasts $\gamma = 0.90$ and $\gamma = 0.80$, respectively, as shown in Figure 5. The resulting topological derivative fields $\mathcal{T}^*(x)$ are presented in Figures 6(a) and 6(b) for Kirchhoff and Reinssner-Midlin plate models, respectively. As expected, the topological derivative is more negative in the neighborhood of the hidden damages. The damage with higher contrast ($\gamma = 0.80$) becomes more evident as also expected.

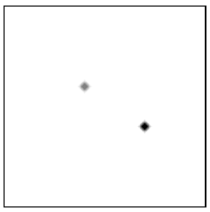

FIGURE 5. Example 2: Target $\omega^\star$ to be reconstructed given by two simultaneous circular damages with radius 0.02m at the positions $(0.40, 0.60)$ and $(0.70, 0.40)$, endowed with different contrasts $\gamma = 0.90$ and $\gamma = 0.80$, respectively.

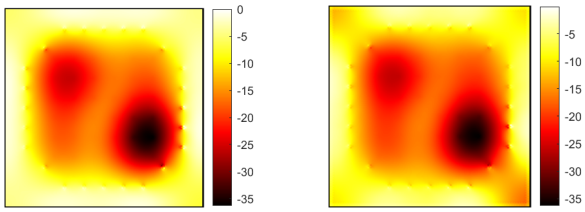

(a) (b)

FIGURE 6. Example 2: Obtained result for Kirchhoff (a) and Reissner-Mindlin (b) plate models by considering 24 sensors distributed as in Figure 2(b).

3.3. **Example 3: Identification of two simultaneous damages of same sizes endowed with high contrast.** In this example, we consider the identification of two simultaneous circular damages of the same sizes and high contrast. In particular, the damages have radius 0.02m and centers at $(0.40, 0.60)$ and $(0.70, 0.40)$ with high contrast $\gamma = 0.01$, as shown in Figure 7. Finally, as explained in the beginning of this section, the measurements computed in a finer mesh are corrupted with White Gaussian Noise (WGN) of varying levels. The obtained topological derivative fields $\mathcal{T}^*(x)$ for 0%, 4%, 8% and 16% of WGN are presented in Figures 8 and 9 for Kirchhoff and Reissner-Mindlin plate models, respectively. From an analysis of these figures, we observe that the two damages are clearly identified even in the presence of noise. For 16% of noise, the result is rather degraded, nevertheless it is still possible to identify the damaged region.

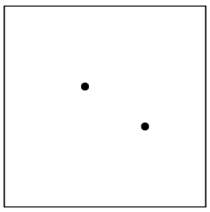

FIGURE 7. Example 3: Target $\omega^\star$ to be reconstructed given by two simultaneous circular damages with radius 0.02m at the positions $(0.40, 0.60)$ and $(0.70, 0.40)$, respectively, both with high contrast $\gamma = 0.01$.

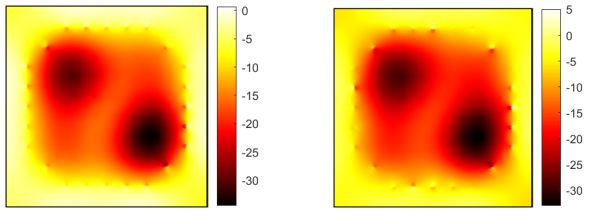

(a) 0% (b) 4%

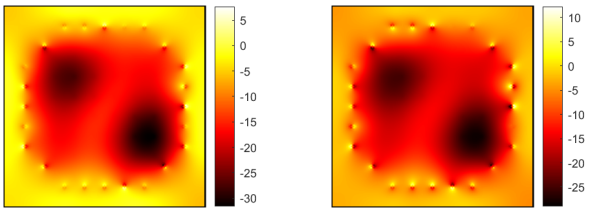

(c) 8% (d) 16%

FIGURE 8. Example 3: Obtained result with noisy data for Kirchhoff plate model by considering 24 sensors distributed as in Figure 2(b).

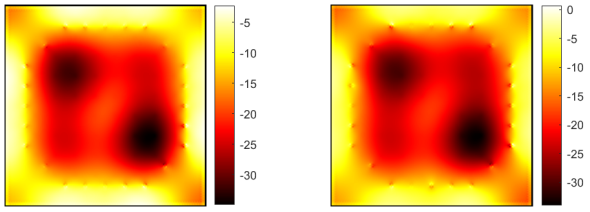

(a) 0% (b) 4%

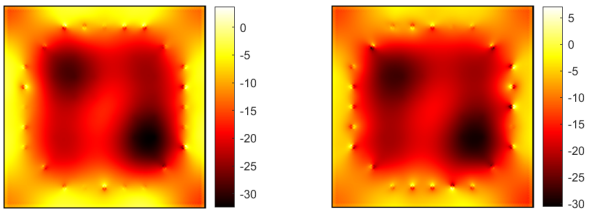

(c) 8% (d) 16%

FIGURE 9. Example 3: Obtained result with noisy data for Reissner-Mindlin plate model by considering 24 sensors distributed as in Figure 2(b).

3.4. **Example 4: Identification of three simultaneous damages of varying shapes endowed with low contrast.** In this example, the identification of three simultaneous damages of the same contrast and different shapes and sizes are considered, as shown in Figure 10. As before, the measurements are computed in a finer mesh and also corrupted with White Gaussian Noise (WGN) of varying levels. The obtained topological derivative fields $\mathcal{T}^*(x)$ for 0%, 8%, 16% and 32% of WGN are presented in Figures 11 and 12 for Kirchhoff and Reissner-Mindlin plate models, respectively. From an analysis of these figures, we observe that the three damages are well identified even in the presence of high level of noise. As point out in the paper by Louër and Rapún (2019), the multi-frequency topological derivative approach is extremely resilient with respect to noisy data.

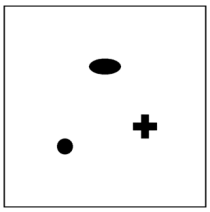

FIGURE 10. Example 4: Target $\omega^\star$ to be reconstructed given by three simultaneous damages of varying shapes and sizes, with contrast $\gamma = 0.90$.

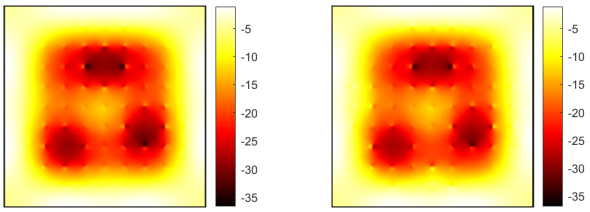

(a) 0% (b) 8%

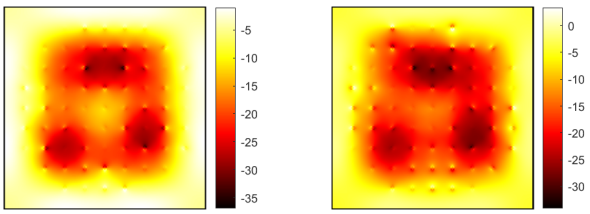

(c) 16% (d) 32%

FIGURE 11. Example 4: Obtained result with noisy data for Kirchhoff plate model by considering 69 sensors distributed as in Figure 2(c).

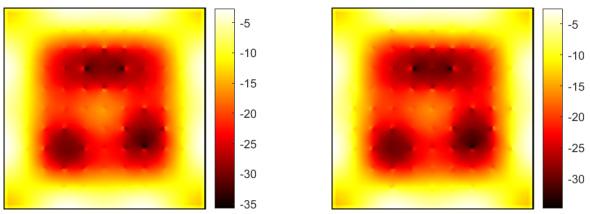

(a) 0% (b) 8%

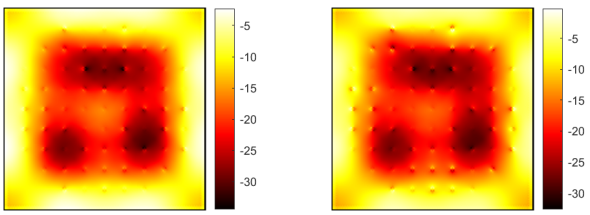

(c) 16% (d) 32%

FIGURE 12. Example 4: Obtained result with noisy data for Reissner-Mindlin plate model by considering 69 sensors distributed as in Figure 2(c).

4. Conclusions

In this paper, a novel approach for solving damage detection and localization problem in Kirchhoff and Reissner-Mindlin plate bending models has been proposed. The topological derivative method is used to minimize a tracking-type shape functional with respect to the geometrical support of the unknown damage distribution. More precisely, the associated topological derivative field is evaluated by using a simple post-processing procedure. As expected, the more $\mathcal{T}(x)$ is negative, the more likely $x \in D$ is within the damage region $\omega^\star \subset D$, given qualitative information on the identification of the damaged zone.

Numerical experiments are presented showing different features of the proposed methodology. In Examples 1, 2 and 3 only 24 sensors are located around the damages, whereas in Example 4 there are 69 sensors uniformly distributed within the domain. Moreover, in Examples 3 and 4 a finer mesh is used to produce the synthetic measurements which are also corrupted with WGN of varying levels. In particular, the identification of two simultaneous circular damages of different sizes with very low contrast ($h_1 = 0.99h_0$) and of same sizes and different contrasts ($h_1 = 0.9h_0$ and $h_1 = 0.8h_0$) are respectively considered in Examples 1 and 2. In Example 3, the identification of two simultaneous damages of same sizes with very high contrast ($h_1 = 0.01h_0$) has been considered. Finally, in Example 4, we deal with the identification of three simultaneous damages of varying shapes and sizes, endowed with low contrast ($h_1 = 0.9h_0$).

Overall, the obtained results are satisfactory, so that the proposed approach can be considered promising in identifying a number of hidden damages in a Kirchhoff and Reissner-Mindlin plate structure from pointwise domain measurements. As an adjacent conclusion, we observed that the results obtained with the Reissner-Mindlin model are slightly better than the ones obtained with the Kirchhoff model. However, the numerical experiments reported in the paper are far to be exhaustive, so that any comparison between both models is only speculative. Finally, our approach induces a level-set method representation of the solution to the inverse problem, which can be combined with well-established and more computationally sophisticated iterative methods, such as the ones reported by Baumeister and Leitão (2005); Burger (2001); Hintermüller and Laurain (2008); Isakov et al. (2011); Tricarico (2013).

Acknowledgements

This research was partly supported by CNPq (Brazilian Research Council), CAPES (Brazilian Higher Education Staff Training Agency) and FAPERJ (Research Foundation of the State of Rio de Janeiro). These financial support are gratefully acknowledged. We would like also to thanks the referees for the impressive and nice comments that strongly contribute to improve the final version of the manuscript.

Conflict of interest

The authors declare that they have no conflict of interest.

Replication of results

The authors are agreeable to share the codes and details of results with those who contact them.

References

H. Ammari and H. Kang. *Reconstruction of small inhomogeneities from boundary measurements*. Lectures Notes in Mathematics vol. 1846. Springer-Verlag, Berlin, 2004.

H. Ammari, J. Garnier, W. Jing, H. Kang, M. Lim, K. Sølna, and H. Wang. *Mathematical and statistical methods for multistatic imaging*, volume 2098. Springer, Switzerland, 2013.

S. Amstutz and A. A. Novotny. Topological optimization of structures subject to von Mises stress constraints. *Structural and Multidisciplinary Optimization*, 41(3):407–420, 2010.

S. Amstutz and A. A. Novotny. Topological asymptotic analysis of the Kirchhoff plate bending problem. *ESAIM: Control, Optimisation and Calculus of Variations*, 17(3): 705–721, 2011.

J.V. Araújo dos Santos, C.M. Mota Soares, C.A. Mota Soares, and N.M.M. Maia. Structural damage identification in laminated structures using frf data. *Composites Structures*, 67:239–249, 2005.

D. Auroux, L. Jaafar Belaid, and M. Masmoudi. A topological asymptotic analysis for the regularized greylevel image classification problem. *ESAIM Mathematical Modelling and Numerical Analysis*, 41:607–625, 2007.

J. L. Batoz. An explicit formulation for an efficient triangular plate-bending element. *International Journal for Numerical Methods in Engineering*, 18:1077–1089, 1982.

J. Baumeister and A. Leitão. *Topics in inverse problems*. IMPA Mathematical Publications, Rio de Janeiro, 2005.

O. Begambre and E. Laier. A hybrid particle swarm optimization – simplex algorithm (psos) for structural damage identification. *Advances in Engineering Software*, 40:883–891, 2009.

L. J. Belaid, M. Jaoua, M. Masmoudi, and L. Siala. Application of the topological gradient to image restoration and edge detection. *Engineering Analysis with Boundary Element*, 32(11):891–899, 2008.

D. Bernal. Load vectors for damage localization. *Journal of Engineering Mechanics*, 128: 7–14, 2002.

M. Burger. A level set method for inverse problems. *Inverse Problems*, 17:1327–1356, 2001.

A. Canelas, A. Laurain, and A. A. Novotny. A new reconstruction method for the inverse potential problem. *Journal of Computational Physics*, 268:417–431, 2014.

A. Carpio and M-L. Rapún. Topological derivatives for shape reconstruction. In Luis L. Bonilla, editor, *Inverse Problems and Imaging*, pages 85–133. Springer, Berlin, Heidelberg, 2008.

A. Carpio and M-L. Rapún. Hybrid topological derivative and gradient-based methods for electrical impedance tomography. *Inverse Problems*, 28:095010, 2012.

R.A.P. Corrêa, L.T. Stutz, and R.A. Tenenbaum. Identification of structural damage in plates based on a model of continuous damage. *Revista Internacional de Métodos Numéricos para Cálculo y Diseño en Ingenierían*, 32:56–64, 2016.

A.D. Ferreira and A. A. Novotny. A new non-iterative reconstruction method for the electrical impedance tomography problem. *Inverse Problems*, 33(3):035005, 2017.

J. F. Funes, J. M. Perales, M-L. Rapún, and J. M. Manuel Vega. Defect detection from multi-frequency limited data via topological sensitivity. *Journal of Mathematical Imaging and Vision*, 55:19–35, 2016.

B. B. Guzina and I. Chikichev. From imaging to material identification: a generalized concept of topological sensitivity. *Journal of the Mechanics and Physics of Solids*, 55 (2):245–279, 2007.

B. B. Guzina and F. Pourahmadian. Why the high-frequency inverse scattering by topological sensitivity may work. *Proceeding of the Royal Society A: Mathematical, Physical and Engineering Sciences*, 471(2179):20150187, 2015.

M. Hintermüller and A. Laurain. Electrical impedance tomography: from topology to shape. *Control and Cybernetics*, 37(4):913–933, 2008.

F. Ihlenburg and I. Babuška. Finite element solution of the Helmholtz equation with high wave number part i: The h-version of the FEM. *Computers & Mathematics with Applications*, 30(9):9–37, 1995. doi: 10.1016/0898-1221(95)00144-N.

V. Isakov, S. Leung, and J. Qian. A fast local level set method for inverse gravimetry. *Communications in Computational Physics*, 10(4):1044–1070, 2011. ISSN 1815-2406. doi: 10.4208/cicp.100710.021210a.

I. Katili. A new discrete Kirchhof-Mindlin element based on Mindlin-Reissner plate theory and assumed shear strain fields. Part i: An extended DKT element for thick-plate bending analysis. *International Journal for Numerical Methods in Engineering*, 36(11): 1859–1883, 1993.

C.G. Koh, B. Hong, and C.Y. Liaw. Substructural and progressive structural identification methods. *Engineering Structures*, 25:1551–1563, 2003.

J.J. Lee, J. W. Lee, J.H. Yi, C.B. Yun, and H.Y. Jung. Neural networks-based damage detection for bridges considering errors in baseline finite element models. *Journal of Sound and Vibration*, 280:555–578, 2005.

U. Lee, K. Cho, and J. Shin. Identification of orthotropic damages within a thin uniform plate. *International Journal of Solids and Structures*, 40:2195–2213, 2003.

C. Liang, F.P. Sun, and C.A. Rogers. Coupled electro-mechanical analysis of adaptive material systems - determination of the actuator power consumption and system energy transfer. *Journal of Intelligent Material Systems and Structures*, 5:12–20, 1994.

F. L. Louër and M. L. Rapún. Detection of multiple impedance obstacles by non-iterative topological gradient based methods. *Journal of Computational Physics*, 388:534–560, 2019.

L. Majumder and C.S. Manohar. A time-domain approach for damage detection in beam structures using vibration data with a moving oscillator as an excitation source. *Journal of Sound and Vibration*, 268:699–716, 2003.

V. G. Maz'ya, S. A. Nazarov, and B. A. Plamenevskij. *Asymptotic theory of elliptic boundary value problems in singularly perturbed domains. Vol. I*, volume 111 of *Operator Theory: Advances and Applications*. Birkhäuser Verlag, Basel, 2000. Translated from the German by Georg Heinig and Christian Posthoff.

P. Monk. *Finite Element Methods for Maxwell's Equations*. Numerical Mathematics and Scientific Computation. Oxford University Press, Oxford, UK, 2003.

S. A. Nazarov and B. A. Plamenevskij. *Elliptic problems in domains with piecewise smooth boundaries*, volume 13 of *de Gruyter Expositions in Mathematics*. Walter de Gruyter & Co., Berlin, 1994.

A. A. Novotny and J. Sokołowski. *Topological derivatives in shape optimization*. Interaction of Mechanics and Mathematics. Springer-Verlag, Berlin, Heidelberg, 2013. doi: 10.1007/978-3-642-35245-4.

A. A. Novotny and J. Sokołowski. *An introduction to the topological derivative method*. Springer Briefs in Mathematics. Springer Nature Switzerland, 2020. doi: 10.1007/978-3-030-36915-6.

A. A. Novotny, R. A. Feijóo, E. Taroco, and C. Padra. Topological sensitivity analysis for three-dimensional linear elasticity problem. *Computer Methods in Applied Mechanics and Engineering*, 196(41–44):4354–4364, 2007.

A.K. Pandey and M. Biswas. Damage detection in structures using changes in flexibility. *Journal and Sound and Vibration*, 169:3–17, 1994.

A.K. Pandey, M. Biswas, and M.M. Samman. Damage detection from changes in curvature mode shapes. *Journal and Sound and Vibration*, 145:321–332, 1991.

G. Park and D.J. Inman. Structural health monitoring using piezoelectric impedance measurements. *Philosophical Transactions of The Royal Society A*, 365:373–392, 2007.

W. K. Park. Multi-frequency topological derivative for approximate shape acquisition of curve-like thin electromagnetic inhomogeneities. *Journal of Mathematical Analysis and Applications*, 404:501–518, 2013.

W. K. Park. Performance analysis of multi-frequency topological derivative for reconstructing perfectly conducting cracks. *Journal of Computational Physics*, 335:865–884, 2017.

M. Pena and M. L. Rapún. Application of the topological derivative to post-processing infrared time-harmonic thermograms for defect detection. *Journal of Mathematics in Industry*, 10(4):1–25, 2020.

A. Quarteroni and A. Valli. *Numerical Approximation of Partial Differential Equations*. Springer-Verlag, Berlin, Heidelberg, 1997.

M.A. Rao, J. Srinivas, and B.S.N. Murthy. Damage detection in vibrating bodies using genetic algorithms. *Computers and Structures*, 82:963—968, 2004.

A. Rytter. *Vibrational Based Inspection of Civil Engineering Structures*. Ph.D. Thesis, Dept. of Building Technology and Structural Engineering, Aalborg University, Denmark, 1993.

O.S. Salawu and C. Williams. Bridge assessment using forced-vibration testing. *Journal of Structural Engineering*, 121:161–173, 1995.

V. Sales, A. A. Novotny, and J. E. Muñoz Rivera. Energy change to insertion of inclusions associated with the Reissner-Mindlin plate bending model. *International Journal of Solids and Structures*, 59:132–139, 2015.

S. Sandesh and K. Shankarb. Damage identification of a thin plate in the time domain with substructuring-an application of inverse problem. *International Journal of Applied Science and Engineering*, 7:79–93, 2009.

J. Shin, J. P. Spicer, and J. A. Abell. Inverse and direct magnetic shaping problems. *Structural and Multidisciplinary Optimization*, 46:285–301, 2012.

J. Sokołowski and A. Żochowski. On the topological derivative in shape optimization. *SIAM Journal on Control and Optimization*, 37(4):1251–1272, 1999.

L.T. Stutz, D.A. Castello, and F.A. Rochinha. A flexibility-based continuum damage identification approach. *Journal of Sound and Vibration*, 279:641–667, 2005.

L.T. Stutz, R.A. Tenenbaum, and R.A.P. Corrêa. The differential evolution method applied to continuum damage identification via flexibility matrix. *Journal of Sound and Vibration*, 345:86–102, 2015.

F.P. Sun, Z. Chaudhry, C. Liang, and C.A. Rogers. Truss structure integrity identification using PZT sensor-actuator. *Journal of Intelligent Material Systems and Structures*, 6: 134–139, 1995.

R.A. Tenenbaum, L.T. Stutz, and K.M. Fernandes. Damage identification in bars with a wave propagation approach: Performance comparison of five hybrid optimization methods. *Shock and Vibration*, 20:863–878, 2013.

R. Tokmashev, A. Tixier, and B. B. Guzina. Experimental validation of the topological sensitivity approach to elastic-wave imaging. *Inverse Problems*, 29:125005, 2013.

A. Tomaszewska. Influence of statistical errors on damage detection based on structural flexibility and mode shape curvature. *Computers and Structures*, 88:154–164, 2010.

P. Tricarico. Global gravity inversion of bodies with arbitrary shape. *Geophysical Journal International*, 195(1):260–275, 2013.

N. Van Goethem and A. A. Novotny. Crack nucleation sensitivity analysis. *Mathematical Methods in the Applied Sciences*, 33(16):1978–1994, 2010.

M. Xavier, N. Van Goethem, and A. A. Novotny. Hydro-mechanical fracture modeling governed by the topological derivative method. *Computer Methods in Applied Mechanics and Engineering*, 365:112974, 2020.

Laboratório Nacional de Computação Científica LNCC/MCTI, Coordenação de Métodos Matemáticos e Computacionais, Av. Getúlio Vargas 333, 25651-075 Petrópolis - RJ, Brasil

Email address: {andressa,novotny}@lncc.br